Separating Hofmeister Trends in the Stern and Diffuse Layer Structures at a Charged Interface

Nathaniel Tetteh, Shyam Parshotam, Julianne M. Gibbs[*]
[*]*Department of Chemistry, University of Alberta, Edmonton, Alberta, T6G 2G2, Canada*

Abstract

Understanding the role of pH and ions on the electrical double layer (EDL) structure of charged mineral oxide/aqueous interfaces remains crucial in modeling various environmental and industrial processes. Yet the simultaneous contribution of pH and specific ion effects (SIEs) on the different layers of the EDL remains unknown. Here, we utilize zeta potential (ζ) measurements, vibrational sum frequency generation (vSFG), and the maximum entropy method (MEM) to ascertain the detailed structure of water in the Stern and diffuse regions of the EDL at the silica/water interface under varying pH conditions for different alkali chlorides. Both at pH 2, when the surface is nearly neutral, and at pH 12, when the surface is highly charged, we observe that the Li^+ and Na^+ disrupt existing water structures within the Stern layer while Cs^+ enhances them. Moreover, the SIE trends for the diffuse and Stern layers are opposite with respect to one another at pH 2 (in the amount of ordered water) and at pH 12 (in amount of net oriented water). Finally, we observe pH-dependent SIE in ζ, which results in Cs^+ exhibiting the least ordered diffuse layer at low pH and the most at high pH. These results indicate that SIEs play critical yet separable roles in governing both the electrostatic and water structuring capabilities in the EDL at charged surface.

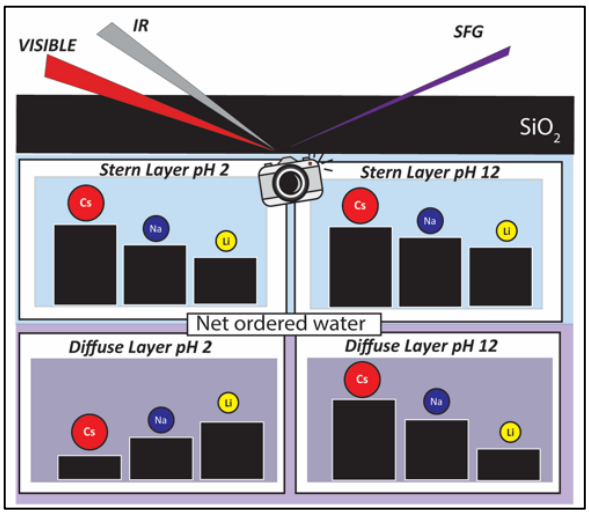

Introduction

The dynamics and structure of the electrical double layer (EDL) formed at the charged silica/aqueous interface have gained considerable attention due to their significance in understanding various biological, technological, and environmental phenomena.[1–3] The EDL is most commonly described by a Stern layer of fixed ions near the solid surface and a diffuse layer of mobile ions based on mean-field theories established by Helmholtz, Guoy-Chapman, Stern and Grahame.[4–8] However, these models fall short at providing a molecular picture of the structure and arrangement of dominant chemical species like water as well as an underlying mechanism of molecular interactions at charged aqueous interfaces. Furthermore, these models often assume trends in specific ion effects for a given solid; in other words for a given ion the capacitance or Stern layer thickness is generally considered to be independent of pH [9] or ion concentration.[10–12] Given the importance of cations in interfacial processes such as adsorption and desorption,[13–15] environmental transport,[16,17] mineral dissolution,[18,19] and surface charge development[20–22] more accurate EDL models and molecular descriptions are needed to be able to predict many environmentally relevant phenomena.

Over the past two decades, techniques such as AFM,[23–26] X-ray spectroscopies,[9,27–29] electrokinetic measurements,[30–32] nonlinear optics,[32–42] and MD-DFT simulations[43–48] have been used to decipher the EDL structure at charged aqueous interfaces under varying physical conditions like pH[34,36], ion concentration,[49] and temperature.[50] Among these techniques, vibrational sum frequency generation (vSFG) has become a leading tool for probing the EDL structure due to its sensitivity to the noncentrosymmetric organization of molecular species at buried interfaces.[39] By measuring the vibrational resonance of water molecules, vSFG is able to provide information about the hydrogen bonding network at charged interfaces. Accordingly, it has been utilized by our group and others to determine how the EDL structure changes depending on the identity of the cation in the aqueous phase.[36,51,52] Yet one limitation of the more common vSFG intensity measurements is difficulty in separating the contributions from the Stern and diffuse layers to the total vSFG EDL spectrum. This difficulty arises as the SF intensity is related to the square modulus of the second order nonlinear susceptibility that provides molecular information about the interface, $|\chi^{(2)}|^2$, making it challenging to deconvolute the different contributions to the total $\chi^{(2)}$ response.

To overcome this challenge, our group has utilized vSFG, electrokinetic measurements, and the maximum entropy method (MEM) with reference phase-sensitive vSFG and heterodyned second harmonic generation (HD-SHG) data to determine the complex spectra of $\chi^{(2)}$ and deconvolute the various spectral components of the EDL.[53–55] This approach has revealed that the Stern layer at the silica/water interface is made up of different water populations whose net orientation and extent of ordering is sensitive to ion concentration[53] and pH dependent.[54] In contrast the diffuse layer exhibits no net reorientation upon changing the salt or pH from pH 2 to 12.[54,55] A recent heterodyned SFG study yielded a similar molecular interpretation of the pH-

dependent evolution of the EDL indicating that our MEM-based analysis was accurately capturing the interfacial structure.[56]

While efforts to separate the different regions of the EDL are more recent, researchers have long been interested in the role of ion identity on the overall interfacial structure.[20,57–59] At the silica interface, previous vSFG studies focused on the entire EDL have revealed that identity of the alkali ion does affect the EDL structure[37] and that the effects are highly dependent on pH.[36] However, the combined effect of ion identity and pH on the structure of the Stern layer adjacent to the solid has not been determined. Recently, Hunger et al.[60] performed phase-sensitive SFG accompanied by MD-DFT simulations and concluded that specific ion effects observed near neutral pH at high salt concentrations (1 M) in the vSFG complex spectra of the EDL arose primarily from the Stern layer. The authors argued that under these conditions the surface electric field is restricted to the structure of the silica and independent of the electrolyte, while the individual fields coming from the ions and the water are ion-specific and compensate each other rendering the total electric field invariant to the nature of the ion.[60] However, ion-specific differences have been observed in surface potentials,[11] zeta potentials (ζ),[61] and surface force[62] measurements, albeit at lower salt concentrations, suggesting that the diffuse layer structure, which is dominated by electrostatic interactions should be influenced by the specific ion. Moreover, this study conducted at one pH did not reveal the pH evolution of the Stern layer, which has been found to vary significantly for silica in the presence of sodium ions.[54,55]

In this work we have separated the response of the Stern layer and diffuse layer to identify their respective pH-dependent specific ion effects using our combined experimental approach with MEM analysis. Firstly, we found ζ exhibited an inversion in ion specific trend at lower versus higher pH in the presence of alkali chlorides. Such pH-dependent specific ion effects had not been

previously reported using electrokinetic measurements despite the abundance of specific ion measurements on colloids.[31,61] Secondly, using our deconvolution approach, we determined that the cation identity separately impacts the water structure in the diffuse and the Stern layers. Specifically, near the point of zero charge (pH 2) we observed opposite trends in the amount of net ordered water for the Stern and diffuse layers. Finally, as the pH was increased, the specific ion trend in the diffuse layer structure inverted based on the pH-dependence of ζ. In contrast, within the Stern layer at both low and high pH, we observed that the more chaotropic Cs+ leads to greater net ordering of water than Na^+ and Li^+. In particularly. Cs^+ promotes hydrogen bonding between water layers at the interface more so than the kosmotropic Na^+ and Li^+. These results suggest that both regions of the EDL are highly sensitive to ion identity and pH yet are decoupled from one another allowing for opposite trends, highlighting the importance of introducing molecular insight into empirical mean field models of the EDL.

Results and Discussion

Measuring the pH-dependent SIE for vSFG and ζ

Sum frequency generation reports on the noncentrosymmetric molecular structure afforded by the charged interface. [63] In our experiments, SFG was achieved by the spatial and temporal overlap of a narrow visible and broad IR pulsed laser light fields at the interface of the silica substrate and the aqueous medium (Figure 1). The IR light was tuned to be in resonance with the vibrational modes of water molecules at the interface within the O-H stretching region allowing us to measure the net orientation and hydrogen-bonded structure of the interfacial water layer.[63] The SFG intensity, I_{SFG}, is given by:

$$I_{SFG} \propto \left|\chi^{(2)}_{total}\right|^2 = |\chi^{(2)}_s + \chi^{(2)}_{DL}|^2 \quad (1)$$

$$\chi^{(2)}_{DL} = \chi^{(3)} \int_{OHP}^{\infty} E_0(z) e^{i\Delta kz} \approx \chi^{(3)} \Phi_{OHP} \quad (2)$$

where, $\chi^{(2)}_{total}$, $\chi^{(2)}_s$, and $\chi^{(2)}_{DL}$ are the total EDL, Stern layer, and diffuse layer second-order susceptibilities, respectively.[54,64] At >10 mM ionic strength, the SFG response in the diffuse layer of the EDL, $\chi^{(2)}_{DL}$, can be approximated as the product of the third-order susceptibility of water $\chi^{(3)}$ and the potential at the outer Helmholtz plane (Φ_{OHP}). The Φ_{OHP} is usually approximated as ζ,[11] which we can measure by streaming current.

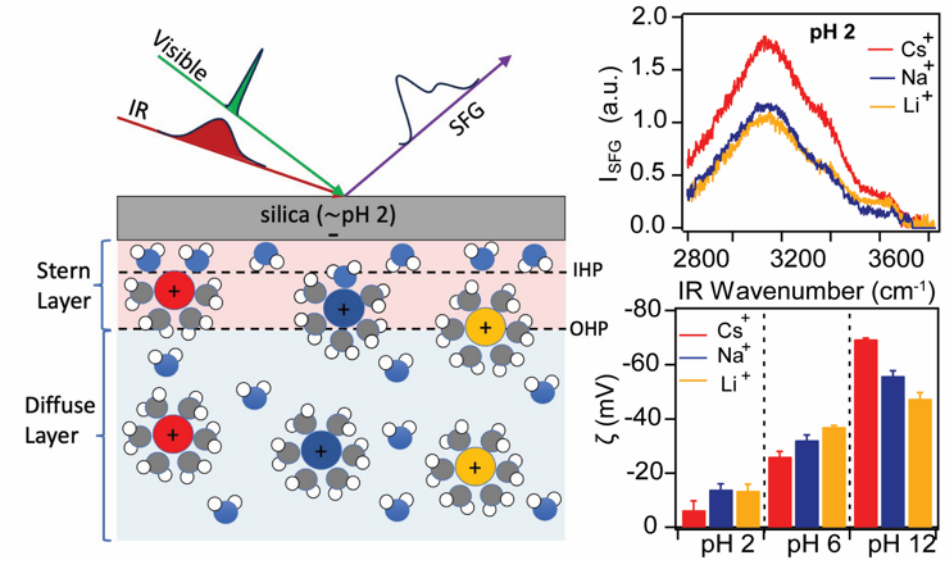

Figure 1. Scheme illustrating specific ion effects in the EDL structure revealed by broadband vibrational sum frequency generation (vSFG). The intensity spectra at the silica/alkali chloride aqueous interface is shown for pH 2, where the silica is slightly negatively charged. For comparison, the pH-dependent ζ was determined from streaming current measurements on planar silica under similar conditions.

The SF intensity spectra are shown for the silica/water interface in the presence of 50 mM alkali chloride under acidic pH conditions with varying alkali cation (Figure 1). Generally, we see three different peaks at 3200, 3400, and 3650 cm^{-1} modes. The first two modes are attributed in

part to interfacial water with a stronger and weaker hydrogen bonding network, respectively, while the small peak at 3650 cm^{-1} is attributed to isolated silanol groups[65] or water experiencing a hydrophobic environment.[66] A Fermi-resonance from the overtone of the water bend also contributes in the 3200 cm^{-1} range.[55,67] For all three of the alkali chloride solutions, the highest intensity was observed at pH 12 (Figure S1), which is consistent with the increased magnitude of the surface charge density at this pH[20,49] and in turn the more negative outer Helmholtz potential due to deprotonation of silanols. Furthermore, at pH 2 the intensity was slightly increased relative to ~pH 6 despite the lower surface charge density expected at pH 2 (near the point of zero charge) (Figure 1 vs S1, respectively). In previous work for the aqueous Na^+/silica interface, an increase in SF intensity at pH 2 was attributed to a flip in the orientation of water molecules in the Stern layer upon decreasing the pH from pH 2 to neutral pH.[34,38]

Next, we measured ζ using streaming current measurements on planar silica (Figure 1). We observed that under neutral and acidic conditions the Cs^+ exhibits the lowest magnitude ζ compared to Na^+ and Li^+ but the trend inverts at higher pH. This pH dependence in the specific ion effects of ζ by electrokinetic measurements has not been previously reported, but it is consistent with surface force measurements at the silica aqueous alkali chloride interface near neutral pH and pH 9 where an inversion in trend was also observed for the determined F_{OHP}.[62] These vSFG and streaming current results support that specific ion effects in both ζ and total EDL structure are highly pH dependent. Yet how the pH dependence of the specific ion trends manifests in the separate regions of the EDL (the Stern layer and the diffuse layer) is unclear. To address this, we require knowledge of the complex spectra $\chi^{(2)}_{total}$ from the overall intensity to properly deconvolute the Stern and diffuse layers contributions (equation 1).[53,64,68]

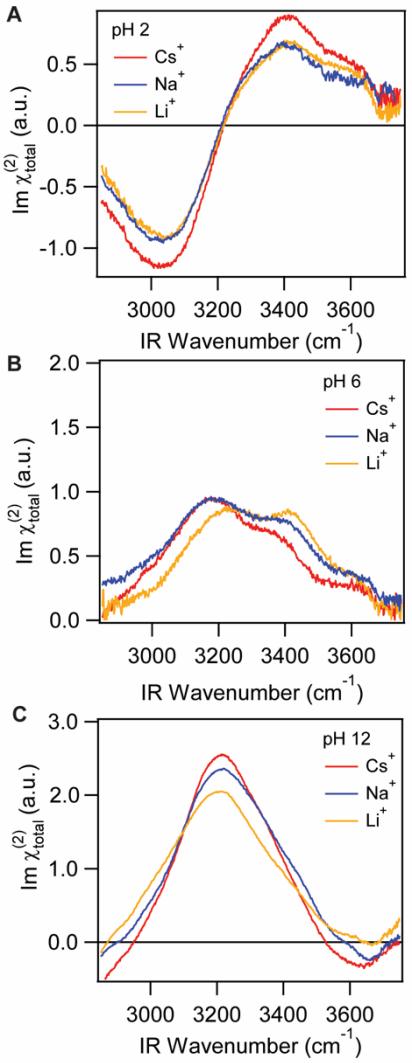

Figure 2. The imaginary component of the complex spectra of $\chi^{(2)}_{\text{total}}$ from the silica/ 50 mM alkali chloride aqueous interface at (A) pH 2, (B) pH 6, and (C) pH 12.

To do this, we employed the maximum entropy method (MEM)[69,70] to determine the magnitude of the SF response and the relative phase of the different oscillators (water molecules) in our spectrum. Additionally, in our analysis we need the error phase, the phase offset between the relative MEM phase and the absolute phase. Our previous work has shown that the pH-dependence of the error phase can be predicted from heterodyned second harmonic generation (HD-SHG), a complementary nonlinear measurement.[53,55] Recent work examining specific ion effects in HD-SHG experiments did not observe statistically significant differences in the HD-

SHG phase with varying alkali ion.[33] As such we assume that the error phase would be similar for each 50 mM alkali solution for a given pH. Using the previously reported error phase spectra determined at ~pH 2, 6 and 12 for the silica/aqueous interface with Na^+ (Figure S4) [53,71] and the MEM analysis of our intensity spectra, we generated the imaginary spectra, $Im\chi^{(2)}_{total}$, which can be related to the net orientation of the water molecules in the whole EDL based on the sign of $Im\chi^{(2)}_{total}$.

The positive and negative features indicate the presence of populations of water molecules oriented with hydrogens towards the surface and away from the surface, respectively (Figure 2).[71] For pH 2, the $Im\chi^{(2)}_{total}$ spectra show a negative feature around ~3000 cm^{-1} and a positive feature for both 3400 cm^{-1} and 3600 cm^{-1} (Figure 2A). However, near neutral pH and at pH 12, the negative feature at 3000 cm^{-1} became positive and blue-shifted with increasing amplitude as the pH was increased (Figure 2B and C). Additionally, the 3400 cm^{-1} mode increased in amplitude while remaining positive with increasing pH. Finally, at 3600 cm^{-1} the amplitude transitioned from positive to negative as pH increased. To examine the impact of the different ions on the Stern and diffuse layer structures we now need to deconvolute these $Im\chi^{(2)}_{total}$ spectra aided by the corresponding ζ measurements.

We begin by first determining the contribution of the diffuse layer to the total complex spectra (i.e. $\chi^{(3)}\Phi_{OHP}$), using the $\chi^{(3)}$ spectrum from our previous work[53] and approximating Φ_{OHP} as ζ from our streaming current measurements. The $\chi^{(3)}$ spectrum reports on the water in the diffuse layer that is aligned or polarized by the outer Helmholtz potential. Consequently $\chi^{(3)}$ has been shown to be independent of the solid and the salt concentration at less than 100 mM.[72] We then subtracted $Im\chi^{(3)}\Phi_{OHP}$ from the complex spectra $Im\chi^{(2)}_{total}$ to obtain the Stern layer spectra

$Im\chi_S^{(2)}$ at each pH (Figure 3A-C, eq. 1-2). The corresponding diffuse layer spectra are shown in Figure 3D-F. As is immediately evident, both the Stern layer and diffuse layer spectra exhibit significant specific ion effects that are also pH dependent. The minimum amplitude for the Stern layer is observed at pH 6 while for the diffuse layer spectra it is observed at pH 2 (Figure 3B and D, respectively). Thus, the nonmonotonic trend with increasing pH observed for the intensity spectra can be attributed to the trend in the $Im\chi_S^{(2)}$ spectra as we move from pH 2 to 12 (Figure 3A-C), which also reveals a flip in orientation of much of the water in the Stern layer (change in sign of $Im\chi_S^{(2)}$). On the other hand, the $Im\chi_{DL}^{(2)}$ increases and remains positive throughout the pH range due to the increasing magnitude of the interfacial potential that aligns the diffuse layer.

pH-Dependent Specific Ion Effects on Stern Layer Water Structure.

Previous work at the silica/water interface revealed that at higher pH, the water in the Stern layer experienced a hydrogen-bonding environment that broke the C_{2v} symmetry of the water, such that each OH behaved as an individual oscillator.[55,73] At lower pH, this generally held true although a bit of C_{2v} character appeared in water near pH 2.[55] With this in mind, at neutral and high pH the imaginary spectra of the Stern layer can be interpreted where the negative modes represent decoupled OH oscillators of water with hydrogen atoms facing away from the surface and positive modes being OH oscillators with H towards the surface. At pH 2, the situation is slightly altered where the sign of $Im\chi_S^{(2)}$ reports on the direction of the dipole moment of the water rather than the individual OH bonds. [54,71] We now consider the effect of specific ions on the Stern layer water structure at acidic, near neutral, and basic conditions (Figure 3). Figure 4 highlights the different water populations based on our peak assignments and the respective positions of the cations at the different pH for Cs^+ and Li^+.

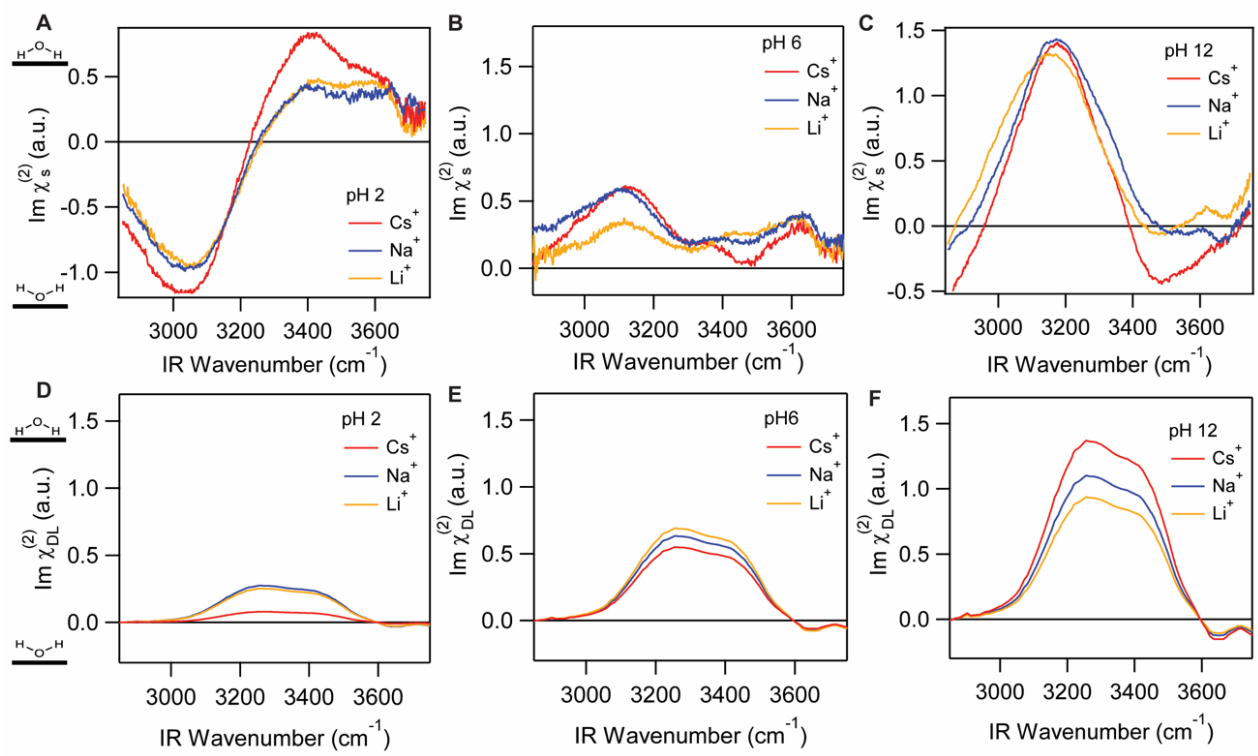

Figure 3. The imaginary component of the Stern (A-C) and diffuse (D-F) layer water ($\chi^{(2)}$) spectra for the silica/ 50 mM alkali chloride aqueous interface at pH 2 (A and D), pH 6 (B and E), and pH 12 (C and F). The sum of the Stern and diffuse layers is equal to the total EDL ($Im\chi^{(2)}_{total}$) spectra shown in Figure 2.

For the nearly neutral silica surface at pH 2 (Figure 3A), the spectra are consistent with water molecules acting as a hydrogen acceptor from the silanols (positive mode at 3100 cm^{-1}) as well as a hydrogen bond donor to the silanol groups (negative mode at 3400 cm^{-1}). The decrease in amplitude of both modes follows the order $Cs^+ > Li^+ \approx Na^+$ suggesting that the kosmotropic ions (Li^+, Na^+) disrupt the exiting hydrogen bonding network at the surface. while the chaotropic ion (Cs^+) with small hydration shell promotes order in the interfacial water structure despite it being closer to the interface (as previous studies have shown the Stern layer thickness is proportional to the magnitude of ζ)[49] (Figure 4). Yet the positions of the various peaks do not shift irrespective of the ion suggesting that the formation of the various H-bonded water environments is less dependent on the ion identity as compared to the pH.

At near neutral pH (~pH 6) in the presence of 50 mM alkali chloride, the silica surface becomes charged due to deprotonation of surface silanols resulting in significant changes to the Stern layer structure. For all three alkali ions, upon increasing the pH from 2 to 6 we see a flip in the orientation of the water molecules in the strong H-bond network and a gradual decrease in amplitude of the weak H-bonded network (Figure 3B). We have attributed this net flip to the loss of water acting as a hydrogen-bond acceptor to surface silanols and the increase in water acting as a hydrogen bond donor to charged sites. This preference for orienting as a hydrogen-bond donor stems from the attractive interactions that exists between the negative electric field from the charged surface and the direction of the water dipole.[54]

For pH 12, the main feature is a positive peak at 3100 cm^{-1} attributed to water molecules donating H-bond to the siloxide sites at the highly deprotonated surface (Figure 3C and Figure 4). For each of the ions there seem to be very little disparity between the amplitude of the 3100 cm^{-1} peak although we see a red shift for Li^+, indicating a stronger H-bond water network in its presence but not a larger amount of ordering. This strengthened interaction is consistent with the concept of matching water affinity[74] where the more hydrated ions like lithium interact strongly with the strongly hydrated siloxide surface. Most striking, however, is the negative mode at 3500 cm^{-1}, which is much more pronounced for Cs^+ than the kosmotropic ions. This mode has been attributed to a water molecule acting as a hydrogen bond donor both to the surface and to the water layer with the latter leading to the negative peak at 3500 cm^{-1} (Figure 4).[73] The fact that this mode is much smaller for Li^+ and Na^+ supports previous MD-DFT and SFG lifetime measurements that Na^+ and Li^+ promote in-plane H-bonding and minimize H-bonding between water layers.[46] Moreover, spectral overlap between this negative peak at 3500 cm^{-1} and the positive peak at 3400 cm^{-1} arising from water donating a hydrogen to neutral silanol sites might explain why the Cs^+

exhibited a minimum in this region for the spectrum at pH 6. At pH 12, the silanol sites that hydrogen bond with water are less abundant contributing less to the Stern layer spectrum allowing this negative mode at 3500 cm^{-1} to appear (Figure 3B and C, respectively).

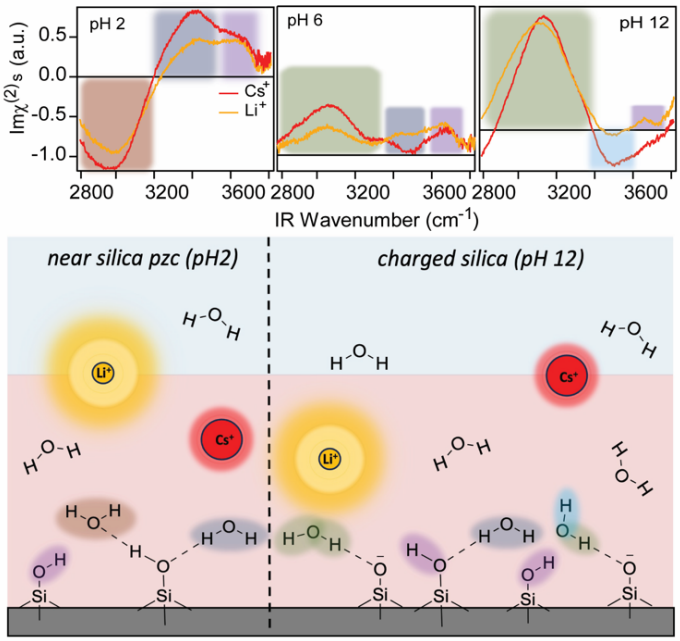

Figure 4. Illustration of the proposed molecular species that contribute to the Stern layer spectra in the presence of Cs^+ vs Li^+. At low pH, the hydrogen-bonding environments are similar, but water is more ordered by Cs^+, which is expected to be closer to the surface. At high pH, we propose that Cs^+ switches its relative position from the surface and promotes hydrogen-bonding along the surface normal between water layers (negative peak at 3500 cm^{-1}).

Finally, the increased extent of hydrogen-bonding between adjacent water layers in the presence of Cs^+ vs Na^+ and Li^+ at pH 12 is consistent with the simulations of Yamakata et al who observed that the density of water at the interface increases as hydrophobic ions approach a negatively charged interface leading to an increase in the band intensity at 3400 cm^{-1}.[75] Moreover, it also helps explain the relative increase in ζ magnitude observed for Cs^+ at pH 12 as an increase in density would lead to an increase in the relative permittivity,[76] which should lead to weaker screening in the Stern layer.[49] Another explanation for the inversion in trend for ζ at high pH is Cs^+ moving further away from the highly charged silica surface owing to weaker interactions with

the well-solvated siloxide sites[77] (Figure 4), which could also lead to greater amounts of ordered water and a larger ζ magnitude.

Specific Ion Effects on H-Bonding Networks, Oriented, and Ordered Water.

To relate the spectral changes in $Im\chi_{DL}^{(2)}$ and $Im\chi_{s}^{(2)}$ to the extent of net ordering and net orientation of water in the different regions of the EDL, we integrated the negative and positive features in each spectrum. An approximation of the amount of net ordered water was determined by adding the absolute values of the negative and positive peak areas, while the net orientation was determined from the sum of the negative and positive peak areas. This analysis allows us to distinguish between water that is highly ordered in specific hydrogen-bonding environments and the net alignment of all water molecules.

Figure 5 exhibits the ion specific trends in the Stern layer compared to the diffuse layer as the pH is varied. The net ordering of water in the Stern layer is generally more pronounced than in the diffuse layer at low and neutral pH (Figure 5A). At pH 12, the electrostatically oriented diffuse layer water becomes more significant such that it exhibits a similar extent of net ordering to that in the Stern layer, which can be attributed to the higher surface charge density leading to a larger outer Helmholtz potential. In contrast, the net orientation of water exhibits a clear pH-dependence for both the Stern and diffuse layers (Figure 5B). At pH 2, near the point of zero charge, there is pronounced ordering of strongly and weakly hydrogen-bonded water populations, but they exhibit opposite orientation (Figure 5C). Accordingly, the net orientation of the Stern layer is small at this pH while the net amount of order is large (Figure 5B and A, respectively).

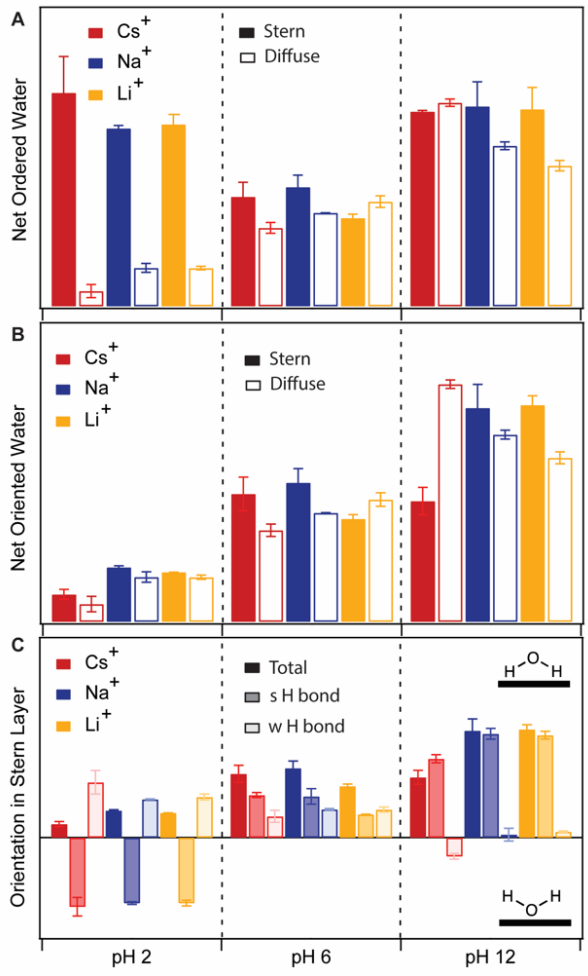

Figure 5. Specific ion trends for the Stern and diffuse layers in the: (A) average amount of net ordered water and (B) the average amount of net oriented water. (C) SIE trends in the net orientation of the Stern layer in terms of total water, the more strongly hydrogen-bonded (s H bond) and more weakly hydrogen-bonded (w H bond) network. The values are the average of integrating two separate SF replicates, and the error bar is the range of measured values.

Regarding specific ion effects, at pH 2 the amount of ordered water exhibits opposite SIEs in the two layers of the EDL with Cs^+ exhibiting the highest amount of ordered water in the Stern layer and the least in the diffuse layer (Figure 5A). However, the net orientation of water in the Stern layer and the diffuse layer exhibits the same SIE trend at pH 2: $Cs^+<Na^+<Li^+$ (Figure 5B). As mentioned, this difference in net ordering vs net orientation for the Stern layer arises from the highly ordered but oppositely oriented strongly and weakly H-bonded species observed at pH 2 with Cs^+ in particular, leading to a well oriented weak H-bond network (Figure 5C). At pH 6, when

the strongly hydrogen-bonded population has flipped within the Stern layer, both the net orientation and net ordering of water in the Stern layer are greater for Cs^+ vs Li^+ while the opposite trend is again observed for the diffuse layer. If we look more closely at the Stern layer structure, we see the most pronounced Hofmeister trends in amplitude for the strong rather than the weak H-bond network (Figure 5C). However, as mentioned this could arise from a negative population at 3400 cm^{-1} that is starting to emerge for Cs^+ owing to hydrogen-bonding between water layers that cancels the response from water acting as a hydrogen bond donor to neutral silanol sites.

Finally, at pH 12 we observe a flip in the SIE with Cs^+ exhibiting the greatest amount of net order in the diffuse layer based on the largest ζ magnitude. Yet for all of the specific cations, a similar extent of order in the Stern layer is observed (Figure 5A). In contrast, the net orientation now reveals pronounced and opposite SIEs for the Stern and diffuse layers (Cs^+<Li^+ vs Li^+<Cs^+, respectively). Similar to pH 2, we propose that the Cs^+ promotes a highly ordered Stern layer at this pH, but with water populations exhibiting opposite orientations leading to an overall decrease in the net orientation compared with the other cations.

Altogether these results suggest that despite changes in ion affinity (based on the trends in ζ potential) and surface hydration with increasing pH, Cs^+ consistently leads to the most amount of net ordering for the water in the Stern layer. However, the net orientation of water can exhibit different trends owing to cancellation of different water populations that are opposite in orientation. Finally, and perhaps most significantly, the Stern layer and diffuse layers can exhibit opposite trends in SIEs revealing that the structures are largely decoupled from one another. Such decoupling of the Stern and diffuse layer has been observed in non-resonant SHG measurements concerning the dynamics but not evaluated in terms of hydrogen-bonded structure.[78] This latter

observation drives home that it is critical to deconvolute the different layers of the EDL to properly understand SIEs at charged oxide aqueous interfaces.

Conclusions

We have studied the simultaneous contribution of specific ion effects and pH on the Stern and diffuse layer water structure at the silica/water interface. Using a combination of complementary techniques: vibrational sum frequency generation, streaming current measurement and the maximum entropy method, we deconvoluted the Stern layer spectra $Im\chi_S^{(2)}$ from the entire EDL in the presence of Li^+, Na^+ and Cs^+ chloride solutions. Near the point of zero charge (pH 2), the Stern and diffuse layer show opposite trends with respect to the specific ions for the amount of ordered water. The more hydrophobic Cs^+ leads to greater water structuring in the Stern layer than Na^+ and Li^+ but exhibits the lowest magnitude of zeta potential leading to less electrostatic ordering manifested in the diffuse layer of the EDL. This trend in Cs^+ promoting more order in the Stern layer compared with Li^+ with opposite effects on the diffuse layer is also exhibited near neutral pH. Under basic conditions, however, the SIEs exhibit a dramatic reverse in trend in ζ indicating that Cs^+ is pushed further away from the interface. Consistent with this observation, we observe signatures in the Stern layer of water hydrogen-bonding between layers for Cs^+ and not the other cations. Decoupling the contributions of each of the specific ions to the pH-evolution of the Stern and diffuse layers provides mechanistic understanding of reversal of Hofmeister trends at the silica/water interface[62,79] as well as greater insight into changes in the Stern layer structure not predicted by current models of the interface. Moreover, these pH dependent SIEs studies serves as a starting point to expand our understanding of important industrial processes involving

oxide/electrolyte interfaces such flotation in mining and extraction[80] and ion exchange in wastewater treatment.[81,82]

Supporting Information

Supporting information includes a detailed description of material preparation, experimental techniques and procedures, replicates of experimental data, discussion of local field effect corrections for the intensity spectra and the frequency-dependent error phase used for each pH.

AUTHOR INFORMATION

Corresponding Author

*E-mail: julianne.gibbs@ualberta.ca

Notes

The authors declare no competing financial interest.

ACKNOWLEDGEMENTS

J.M.G. thank the Natural Sciences and Engineering Research Council of Canada for financial support (Discovery Grants) and the Institute of Oil Sands Innovation for the Surpass Analyzer.

REFERENCES

[1] L. Ban, E. Borguet, G. E. Brown, R. T. Cygan, J. J. Deyoreo, P. M. Dove, M. Gaigeot, F. M. Geiger, J. M. Gibbs, V. H. Grassian, A. G. Ilgen, Y. Jun, N. Kabengi, L. Katz, J. D. Kubicki, J. Lu, C. V Putnis, R. C. Remsing, K. M. Rosso, G. Rother, M. Sulpizi, M. Villalobos, H. Zhang, **2022**, DOI 10.1021/acs.chemrev.2c00130.

[2] E. Leontidis, *Adv Colloid Interface Sci* **2017**, *243*, 8–22.

[3] G. Gonella, E. H. G. Backus, Y. Nagata, D. J. Bonthuis, P. Loche, A. Schlaich, R. R. Netz, A. Kühnle, I. T. McCrum, M. T. M. Koper, M. Wolf, B. Winter, G. Meijer, R. K. Campen, M. Bonn, *Nat Rev Chem* **2021**, *5*, 466–485.

[4] H. von Helmholtz, *Ann Phys* **1853**, *165*, 353–377.

[5] M. Gouy, *J. Phys. Theor. Appl.* **1910**, *9*, 457–468.
[6] D. L. Chapman, *The London, Edinburgh, and Dublin Philosophical Magazine and Journal of Science* **1913**, *25*, 475–481.
[7] O. Stern, **1924**.
[8] D. C. Grahame, *Chem Rev* **2002**, *41*, 441–501.
[9] M. A. Brown, Z. Abbas, A. Kleibert, R. G. Green, A. Goel, S. May, T. M. Squires, *Phys Rev X* **2016**, *6*, 1–12.
[10] D. A. Sverjensky, *Geochim Cosmochim Acta* **2005**, *69*, 225–257.
[11] M. A. Brown, Z. Abbas, A. Kleibert, R. G. Green, A. Goel, S. May, T. M. Squires, *Phys Rev X* **2016**, *6*, 1–12.
[12] D. A. Sverjensky, *Geochim Cosmochim Acta* **2001**, *65*, 3643–3655.
[13] N. Allen, M. L. Machesky, D. J. Wesolowski, N. Kabengi, *J Colloid Interface Sci* **2017**, *504*, 538–548.
[14] N. Allen, C. Dai, Y. Hu, J. D. Kubicki, N. Kabengi, *ACS Earth Space Chem* **2019**, *3*, 432–441.
[15] Y. Kim, R. J. Kirkpatrick, *Geochim Cosmochim Acta* **1997**, *61*, 5199–5208.
[16] R. Huang, C. Ma, Q. He, J. Ma, Z. Wu, X. Huangfu, *Environ Sci Nano* **2019**, *6*, 2712–2723.
[17] A. G. Ilgen, N. Kabengi, K. Leung, P. Ilani-Kashkouli, A. W. Knight, L. Loera, *Environ Sci Nano* **2021**, *8*, 432–443.
[18] G. Berger, E. Cadore, J. Schott, P. M. Dove, *Geochim Cosmochim Acta* **1994**, *58*, 541–551.
[19] F. K. Crundwell, *ACS Omega* **2017**, *2*, 1116–1127.
[20] P. M. Dove, C. M. Craven, *Geochim Cosmochim Acta* **2005**, *69*, 4963–4970.
[21] T. A. Gmür, A. Goel, M. A. Brown, *Journal of Physical Chemistry C* **2016**, *120*, 16617–16625.
[22] M. Karlsson, C. Craven, P. M. Dove, W. H. Casey, *Aquat Geochem* **2001**, *7*, 13–32.
[23] M. L. Schlegel, K. L. Nagy, P. Fenter, N. C. Sturchio, *Geochim Cosmochim Acta* **2002**, *66*, 3037–3054.
[24] U. Sivan, *Curr Opin Colloid Interface Sci* **2016**, *22*, 1–7.
[25] F. Liu, A. Klaassen, C. Zhao, F. Mugele, D. Van Den Ende, *Journal of Physical Chemistry B* **2018**, *122*, 933–946.
[26] B. A. Legg, M. D. Baer, J. Chun, G. K. Schenter, S. Huang, Y. Zhang, Y. Min, C. J. Mundy, J. J. De Yoreo, *J Am Chem Soc* **2020**, *142*, 6093–6102.
[27] Y. Duval, J. A. Mielczarski, O. S. Pokrovsky, E. Mielczarski, J. J. Ehrhardt, *Journal of Physical Chemistry B* **2002**, *106*, 2937–2945.
[28] F. Malloggi, S. Ben Jabrallah, L. Girard, B. Siboulet, K. Wang, P. Fontaine, J. Daillant, *Journal of Physical Chemistry C* **2019**, *123*, 30294–30304.
[29] S. ben Jabrallah, F. Malloggi, L. Belloni, L. Girard, D. Novikov, C. Mocuta, D. Thiaudière, J. Daillant, *Physical Chemistry Chemical Physics* **2017**, *19*, 167–174.
[30] J. Sonnefeld, M. Löbbus, W. Vogelsberger, *Colloids Surf A Physicochem Eng Asp* **2001**, *195*, 215–225.
[31] A. H. Jalil, U. Pyell, *Journal of Physical Chemistry C* **2018**, *122*, 4437–4453.
[32] J. Lützenkirchen, T. Scharnweber, T. Ho, A. Striolo, M. Sulpizi, A. Abdelmonem, *J Colloid Interface Sci* **2018**, *529*, 294–305.
[33] M. D. Boamah, P. E. Ohno, E. Lozier, J. Van Ardenne, F. M. Geiger, *Journal of Physical Chemistry B* **2019**, *123*, 5848–5856.

[34] A. M. Darlington, T. A. Jarisz, E. L. Dewalt-Kerian, S. Roy, S. Kim, M. S. Azam, D. K. Hore, J. M. Gibbs, *Journal of Physical Chemistry C* **2017**, *121*, 20229–20241.
[35] M. Rashwan, B. Rehl, A. Sthoer, A. M. Darlington, M. S. Azam, H. Zeng, Q. Liu, E. Tyrode, J. M. Gibbs, *Journal of Physical Chemistry C* **2020**, *124*, 26973–26981.
[36] E. L. Dewalt-Kerian, S. Kim, M. S. Azam, H. Zeng, Q. Liu, J. M. Gibbs, *Journal of Physical Chemistry Letters* **2017**, *8*, 2855–2861.
[37] Z. Yang, Q. Li, K. C. Chou, *Journal of Physical Chemistry C* **2009**, *113*, 8201–8205.
[38] B. Rehl, M. Rashwan, E. L. Dewalt-Kerian, T. A. Jarisz, A. M. Darlington, D. K. Hore, J. M. Gibbs, *Journal of Physical Chemistry C* **2019**, *123*, 10991–11000.
[39] E. H. G. Backus, J. Schaefer, M. Bonn, *Angewandte Chemie - International Edition* **2020**, 10482–10501.
[40] M. S. Azam, C. N. Weeraman, J. M. Gibbs-Davis, *Journal of Physical Chemistry Letters* **2012**, *3*, 1269–1274.
[41] M. M. Uddin, M. S. Azam, D. K. Hore, *J Am Chem Soc* **2023**, DOI 10.1021/jacs.3c14836.
[42] F. Raji, C. V. Nguyen, N. N. Nguyen, T. A. H. Nguyen, A. V. Nguyen, *J Colloid Interface Sci* **2023**, *647*, 152–162.
[43] S. H. Chen, S. J. Singer, *Journal of Physical Chemistry B* **2019**, *123*, 6364–6384.
[44] Z. Brkljača, D. Namjesnik, J. Lützenkirchen, M. Předota, T. Preočanin, *Journal of Physical Chemistry C* **2018**, *122*, 24025–24036.
[45] M. Sulpizi, M. P. Gaigeot, M. Sprik, *J Chem Theory Comput* **2012**, *8*, 1037–1047.
[46] A. Tuladhar, S. Dewan, S. Pezzotti, F. S. Brigiano, F. Creazzo, M. P. Gaigeot, E. Borguet, *J Am Chem Soc* **2020**, *142*, 6991–7000.
[47] S. Pezzotti, D. R. Galimberti, M. P. Gaigeot, *Physical Chemistry Chemical Physics* **2019**, *21*, 22188–22202.
[48] S. Dewan, V. Carnevale, A. Bankura, A. Eftekhari-Bafrooei, G. Fiorin, M. L. Klein, E. Borguet, *Langmuir* **2014**, *30*, 8056–8065.
[49] M. A. Brown, A. Goel, Z. Abbas, *Angewandte Chemie International Edition* **2016**, *55*, 3790–3794.
[50] M. S. Azam, C. Cai, J. M. Gibbs, E. Tyrode, D. K. Hore, *J Am Chem Soc* **2020**, *142*, 669–673.
[51] K. A. Lovering, A. K. Bertram, K. C. Chou, *Journal of Physical Chemistry C* **2016**, *120*, 18099–18104.
[52] S. C. Flores, J. Kherb, N. Konelick, X. Chen, P. S. Cremer, *Journal of Physical Chemistry C* **2012**, *116*, 5730–5734.
[53] B. Rehl, J. M. Gibbs, *Journal of Physical Chemistry Letters* **2021**, *12*, 2854–2864.
[54] B. Rehl, E. Ma, S. Parshotam, E. L. DeWalt-Kerian, T. Liu, F. M. Geiger, J. M. Gibbs, *J Am Chem Soc* **2022**, DOI 10.1021/jacs.2c01830.
[55] S. Parshotam, B. Rehl, F. Busse, A. Brown, J. M. Gibbs, *The Journal of Physical Chemistry C* **2022**, *126*, 21734–21744.
[56] F. Wei, S. H. Urashima, S. Nihonyanagi, T. Tahara, *J Am Chem Soc* **2022**, 1–17.
[57] J. Lyklema, *Chem Phys Lett* **2009**, *467*, 217–222.
[58] W. Kunz, *Curr Opin Colloid Interface Sci* **2010**, *15*, 34–39.
[59] W. Hua, D. Verreault, Z. Huang, E. M. Adams, H. C. Allen, *J Phys Chem B* **2014**, *118*, 8433–8440.
[60] J. Hunger, J. Schaefer, P. Ober, T. Seki, Y. Wang, L. Prädel, Y. Nagata, M. Bonn, D. J. Bonthuis, E. H. G. Backus, *J Am Chem Soc* **2022**, *144*, 19726–19738.
[61] G. V. Franks, *J Colloid Interface Sci* **2002**, *249*, 44–51.

[62] J. Morag, M. Dishon, U. Sivan, *Langmuir* **2013**, *29*, 6317–6322.
[63] A. G. Lambert, P. B. Davies, D. J. Neivandt, *Appl Spectrosc Rev* **2005**, *40*, 103–145.
[64] Y. C. Wen, S. Zha, X. Liu, S. Yang, P. Guo, G. Shi, H. Fang, Y. R. Shen, C. Tian, *Phys Rev Lett* **2016**, *116*, 1–5.
[65] L. Dalstein, E. Potapova, E. Tyrode, *Physical Chemistry Chemical Physics* **2017**, *19*, 10343–10349.
[66] J. D. Cyran, M. A. Donovan, D. Vollmer, F. S. Brigiano, S. Pezzotti, D. R. Galimberti, M. P. Gaigeot, M. Bonn, E. H. G. Backus, *Proc Natl Acad Sci U S A* **2019**, *116*, 1520–1525.
[67] M. Sovago, R. K. Campen, G. W. H. Wurpel, M. Müller, H. J. Bakker, M. Bonn, *Phys Rev Lett* **2008**, *100*, 1–4.
[68] P. E. Ohno, H. F. Wang, F. M. Geiger, *Nat Commun* **2017**, *8*, 1–9.
[69] M. Sovago, E. Vartiainen, M. Bonn, *Journal of Physical Chemistry C* **2009**, *113*, 6100–6106.
[70] S. Parshotam, B. Rehl, A. Brown, J. M. Gibbs, *Journal of Chemical Physics* **2023**, *159*, DOI 10.1063/5.0172667.
[71] A. Myalitsin, S. H. Urashima, S. Nihonyanagi, S. Yamaguchi, T. Tahara, *Journal of Physical Chemistry C* **2016**, *120*, 9357–9363.
[72] T. Joutsuka, A. Morita, *Journal of Physical Chemistry C* **2018**, *122*, 11407–11413.
[73] S. H. Urashima, A. Myalitsin, S. Nihonyanagi, T. Tahara, *Journal of Physical Chemistry Letters* **2018**, *9*, 4109–4114.
[74] K. D. Collins, *Biophys J* **1997**, *72*, 65–76.
[75] A. Yamakata, E. Soeta, T. Ishiyama, M. Osawa, A. Morita, *J Am Chem Soc* **2013**, *135*, 15033–15039.
[76] D. I. Karpov, D. A. Medvedev, *J Phys Conf Ser* **2016**, *754*, DOI 10.1088/1742-6596/754/10/102004.
[77] S. Hocine, R. Hartkamp, B. Siboulet, M. Duvail, B. Coasne, P. Turq, J. F. Dufrêche, *Journal of Physical Chemistry C* **2016**, *120*, 963–973.
[78] E. Ma, J. Kim, H. Chang, P. E. Ohno, R. J. Jodts, T. F. Miller, F. M. Geiger, *Journal of Physical Chemistry C* **2021**, *125*, 18002–18014.
[79] N. Schwierz, D. Horinek, U. Sivan, R. R. Netz, *Curr Opin Colloid Interface Sci* **2016**, *23*, 10–18.
[80] Z. yong GAO, Z. yi JIANG, W. SUN, Y. sheng GAO, *Transactions of Nonferrous Metals Society of China (English Edition)* **2021**, *31*, 2081–2101.
[81] N. A. A. Qasem, R. H. Mohammed, D. U. Lawal, *NPJ Clean Water* **2021**, *4*, DOI 10.1038/s41545-021-00127-0.
[82] International Atomic Energy Agency, *Technical reports series No.408* **2002**, 115.